

Article

# Regeneration of Pt-Sn/Al<sub>2</sub>O<sub>3</sub> Catalyst for Hydrogen Production through Propane Dehydrogenation Using Hydrochloric Acid

Yi Sun Choi <sup>1</sup>, Kyeongseok Oh <sup>2</sup>, Kwang-Deog Jung <sup>3</sup> , Won-Il Kim <sup>4</sup> and Hyoung Lim Koh <sup>1,\*</sup> 

<sup>1</sup> Department of Chemical Engineering, RCCT, Hankyong National University, 327, Jungang-ro, Anseong, Gyeonggi 17579, Korea; dltjs118@hknu.ac.kr

<sup>2</sup> Chemical and Environmental Technology Department, Inha Technical College, Inha-ro 100, Michuhol-gu, Incheon 22212, Korea; kyeongseok.oh@inhac.ac.kr

<sup>3</sup> Clean Energy Research Center, Korean Institute of Science and Technology, P.O. Box 131, Cheongryang, Seoul 02792, Korea; jkdcacat@kist.re.kr

<sup>4</sup> R&D Business Lab., Hyosung Co., 74 Simin-daero, Dongan-gu, Anyang, Gyeonggi 14080, Korea; wikim@hyosung.com

\* Correspondence: hlkoh@hknu.ac.kr; Tel.: +82-31-670-5410

Received: 14 July 2020; Accepted: 5 August 2020; Published: 7 August 2020



**Abstract:** Compared with dehydrogenation in conventional petroleum refinery processes, relatively pure hydrogen can be produced by propane dehydrogenation (PDH) without innate contaminants like sulfur and metals. Among the existing catalysts for PDH, Pt catalysts are popular and are often used in conjunction with Sn as a co-catalyst. Coke formation is a major concern in PDH, where catalyst regeneration is typically achieved by periodic coke burning to achieve sustainable operation. In this study, Pt-Sn/Al<sub>2</sub>O<sub>3</sub> catalysts were regenerated after coke burning in three stages: mixing the catalyst with liquid hydrochloric acid, drying, and calcining under air atmosphere. In this process, the optimum concentration of hydrochloric acid was found to be 35% *w/w*. HCl treatment was effective for enhancing redispersion of the metal catalysts and aiding the formation of the Pt<sub>3</sub>Sn alloy, which is considered to be effective for PDH reaction. HCl treatment may provide oxychlorination-like conditions under the calcination atmosphere. The characteristics of the catalysts were examined by X-ray diffraction (XRD), transmission electron microscopy (TEM), temperature-programmed reduction (TPR), X-ray photoelectron spectroscopy (XPS), and CO chemisorption.

**Keywords:** hydrochloric acid treatment; propane dehydrogenation; Pt-Sn/Al<sub>2</sub>O<sub>3</sub>; Pt<sub>3</sub>Sn alloy; regeneration

## 1. Introduction

Hydrogen has been produced via various chemical processes and is considered a future alternative energy resource. Among the chemical processes, propane dehydrogenation (PDH) is becoming popular because it produces hydrogen, along with propylene, from propane feedstock. In stoichiometric counts, one mole of propylene as well as one mole of hydrogen can be produced from one mole of propane feed for PDH. The global demand for propylene is up 100 million tons annually, where propylene is used in various areas such as polymers and chemical intermediates [1,2]. Two major catalysts are used in commercial PDH, that is, Pt-Sn and Cr-based catalysts [3–5]. The main drawback of Cr catalysts is the environmental impact, which tends to decrease its usage [6–9]. In other words, Pt catalysts are known to promote the PDH reaction in the presence of co-metals [10–14] and refined supports [15–19]. The PDH reaction is performed at high temperatures (over 550 °C), leading to unfavorable coke formation on the surface of the catalysts [20–22], which causes deactivation. In qualitative studies, coke has been classified as aliphatic, aromatic, and pseudo-graphitic [23]. The effect of the coke quality

on Pt-Sn catalysts was evaluated by assessing the combustion kinetics [24]. When coke on the catalyst was combusted, the metals on the surface of the catalysts spontaneously sintered [25]. In practice, coke deposits on commercial catalysts are caused by contamination with impurities and loss of chlorine compounds. Sintering of the metal reduces the catalyst activity and destabilizes the balance between the metal and alumina [11]. If the catalyst activity falls considerably below that of the fresh catalyst, regeneration steps can be added. The regeneration of coke-contaminated catalysts is important and should be evaluated with accompanying processes, such as coke burning followed by redispersion, reduction, and so on, if necessary. Coke burning is the primary option for coke removal under oxygen atmosphere [26,27]. It was reported that oxygen atmosphere promotes coke removal from metal surfaces [11,28], whereas ozone atmosphere promotes coke removal from alumina supports [29,30]. Alternatively, coke burning under hydrogen atmosphere has also been reported. It was reported that alumina enhances activation of the catalytically active sites, thereby facilitating regeneration of Pt-Sn catalysts in the naphtha reforming process [31]. Various options have been proposed for regenerating Pt-Sn catalysts subsequent to coke burning. Oxidation redispersion as a secondary treatment was also used under oxygen atmosphere and even under ozone atmosphere. In our previous study [32], we reported that oxychlorination treatment was effective in regenerating Pt-Sn/Al<sub>2</sub>O<sub>3</sub> catalysts after the PDH reaction, and we observed that the activity of catalysts containing Pt<sub>3</sub>Sn alloys was improved after oxychlorination treatment.

Regeneration of Pt-Sn/Al<sub>2</sub>O<sub>3</sub> for PDH reaction by oxychlorination has been rarely studied. Meanwhile, reports of study in regeneration of Pt or Pt-Sn catalyst for naphtha reforming by oxychlorination using HCl or dichloropropane include the following. Arteaga et al. [33] reported that recovery of dispersion in Pt/Al<sub>2</sub>O<sub>3</sub> could be attained by oxychlorination as well as recovery of activity in naphtha reforming, but the effect of chlorine during regeneration of Pt-Sn/Al<sub>2</sub>O<sub>3</sub> is less significant, although chlorine has the additional effect of favoring PtSn alloy formation [34] at high metal loadings [35] or greater intimacy between Pt and Sn dispersed on SnO<sub>x</sub>-modified alumina [34,36,37] at low metal loadings [33]. Our study was intended to study the effect of oxychlorination treatment of Pt-Sn catalysts used in propane dehydrogenation reactions. As the Pt-Sn catalyst for propane dehydrogenation is calcined and reduced at a higher temperature than the Pt-Sn catalyst used for the naphtha reforming reaction, the effect on oxychlorination is expected to be different. It is also of interest whether the PtSn alloy reported in the catalyst for the naphtha reforming reaction will be produced or whether other alloy types may be produced. In this study, we investigate the effects of treatment with a liquid chlorine compound at room temperature on the catalyst activity. The treatment includes three stages: immersion into concentrated HCl solution, drying, and calcination, which names to HCl treatment. In commercial processes, gas-phase regeneration is the better option for regeneration because used catalysts can be regenerated in a reaction vessel in a continual process. The main objectives of the hydrochloric acid (HCl) treatment are to achieve economic catalyst redispersion and enhanced catalyst activation. Coke burning option was used as a reference. After drying and calcining the HCl-treated Pt-Sn/Al<sub>2</sub>O<sub>3</sub> catalysts, the Pt dispersion and the role of Sn/SnO<sub>x</sub> in the catalyst are evaluated. The catalysts are characterized by X-ray diffraction (XRD), transmission electron microscopy (TEM), temperature-programmed reduction (TPR), X-ray photoelectron spectroscopy (XPS), and CO-chemisorption.

## 2. Results

### 2.1. Catalyst Performance

Table 1 shows the classification of the catalysts used in this study. The catalysts were regenerated by different techniques such as coke burning and coke burning combined with HCl treatment in different concentrations of HCl. A bimetallic catalyst composed of Pt-Sn on an alumina support was used. As shown in the catalyst codes in Table 1, two different weight percentages of Pt (3 wt.%) and Sn (4.5 wt.%) were used. As a fresh catalyst, impregnated 3Pt4.5Sn/Al<sub>2</sub>O<sub>3</sub> was calcined and

named PtSn-C. Before the first or second run of PDH, the catalysts were reduced with hydrogen. After the first run of PDH for 3 h, the used PtSn-C catalyst was denoted as PtSn-U, and PtSn-B was named after coke burning of PtSn-U. Subsequently, the catalysts were treated with HCl of different concentrations, and these samples were denoted as the PtSn-B-HCl series, from PtSn-B-HCl5 to PtSn-B-HCl35, depending on the concentration of HCl. Note that HCl treatment comprises treatment with HCl solutions at different concentrations, followed by drying and calcination at 600 °C.

**Table 1.** Procedure for catalyst regeneration (dehydrogenated: first reduction + propane dehydrogenation (PDH) reaction).

| Catalyst Code | Treatment                                      |
|---------------|--|
| PtSn-C        | Calcined                                       |
| PtSn-U        | Calcined/dehydrogenation                       |
| PtSn-B        | Calcined/dehydrogenated/coke burning           |
| PtSn-B-HCl5   | Calcined/dehydrogenated/coke burning/HCl (5%)  |
| PtSn-B-HCl15  | Calcined/dehydrogenated/coke burning/HCl (15%) |
| PtSn-B-HCl25  | Calcined/dehydrogenated/coke burning/HCl (25%) |
| PtSn-B-HCl35  | Calcined/dehydrogenated/coke burning/HCl (35%) |

Figure 1 shows the ‘conversion recovery’ data for the catalysts after regenerated by the three different processes. The three regeneration options are coke burning and two cases of HCl treatment at 5% and 35% concentrations. It should be noted that HCl treatment was performed right after coke burning under the same conditions. On the basis of our understanding of the PDH process, we suggest a more appropriate term, that is, conversion recovery, in this work. The data obtained in the first run of PDH are not identical for the different operations. It is easy to understand our experimental protocols from the following examples. Consider two different scenarios. In one scenario, 30% conversion was recorded after 30 min run of PDH, followed by 29% conversion for the second run of PDH after the regeneration treatment. Another scenario is that 29% conversion was recorded after 30 min run of PDH, followed by 28.5% conversion in the second run of PDH after the regeneration treatment. In these cases, which scenario is superior might be confused if we consider the conversion data for the second PDH run. In this case, 29% conversion may appear superior to 28.5% conversion. However, the reality is that the opposite may be true as 28.5% conversion corresponds to 98.2% ( $28.5/29 = 0.982$ ) recovery after the regeneration treatment compared with 96.7% ( $29/30 = 0.967$ ) recovery in the first case. Returning to Figure 1, the recovery for 3Pt4.5Sn-B (coke burning) reached only 0.56 in 3 h of PDH, while the recovery for PtSn-B-HCl5 reached 0.72, and that for PtSn-B-HCl35 was the highest at 0.79. HCl treatment clearly improved the catalyst activity. Figure 2 presents the selectivity recovery data. The selectivity recovery is represented the same as conversion recovery. All the data were within 0.05, which indicates no significant changes in the selectivity recovery for the three catalysts.

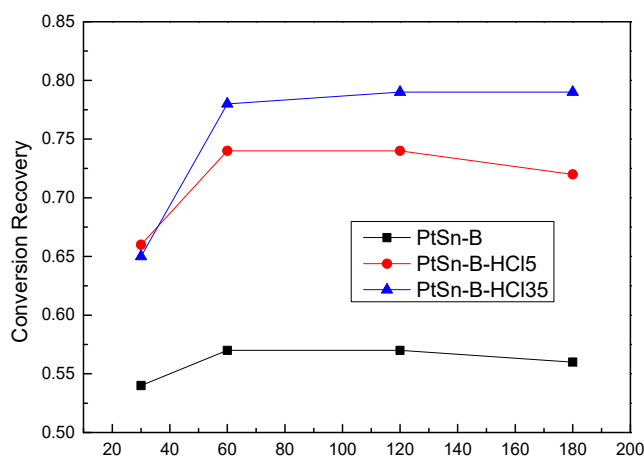


**Figure 1.** Recovery of propane conversion over Pt-Sn/Al<sub>2</sub>O<sub>3</sub>. Reaction conditions—catalyst weight: 0.3 g; reaction temperature: 600 °C; and flow rate: N<sub>2</sub>:H<sub>2</sub>:C<sub>3</sub>H<sub>8</sub> = 70:30:30 (mL/min), WHSV = 11.8 h<sup>-1</sup>.

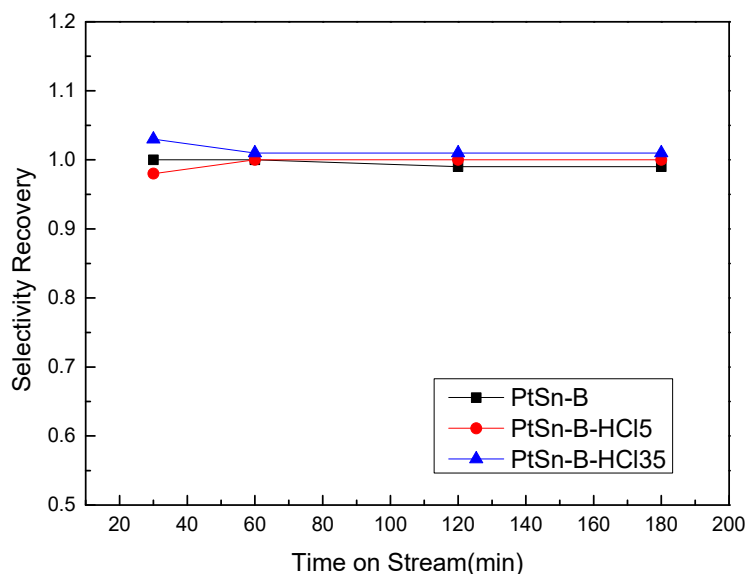


**Figure 2.** Recovery of propylene selectivity of Pt-Sn/Al<sub>2</sub>O<sub>3</sub>. Reaction conditions—catalyst weight: 0.3 g; reaction temperature: 600 °C; and flow rate: N<sub>2</sub>:H<sub>2</sub>:C<sub>3</sub>H<sub>8</sub> = 70:30:30 (mL/min), WHSV = 11.8 h<sup>-1</sup>.

## 2.2. Catalyst Characterization

### 2.2.1. X-Ray Diffraction Analysis

Figure 3 shows the XRD patterns of the 3Pt4.5Sn/Al<sub>2</sub>O<sub>3</sub> catalysts after various treatments. For comparison, the data for the catalysts after hydrogen reduction are also presented. The characteristic XRD peaks of Pt occur at  $2\theta = 41.72^\circ$  and  $46.24^\circ$ . The Pt-Sn alloys in Pt-Sn catalysts often adopt the PtSn and Pt<sub>3</sub>Sn forms. These two alloys would contribute differently to the PDH reaction [38]. The characteristic XRD peaks of the two Pt-Sn alloys were identified separately at  $2\theta = 41.72^\circ$  and  $44.05^\circ$  for the PtSn alloy and  $38.79^\circ$  for the Pt<sub>3</sub>Sn alloy. It should be cautioned that the characteristic peak of the Pt<sub>3</sub>Sn alloy often overlaps with the characteristic peak of alumina. As shown in Figure 3a,b, the characteristic peaks of Pt were observed in the profile of PtSn-C, but these peaks shifted to correspond to those of the PtSn alloy after hydrogen reduction. The particle growth of the PtSn alloy after the PDH reaction (Figure 3c) is attributed to sintering. In general, sintering lowers the degree of Pt dispersion and increases the size of the Pt particles. After the PDH reaction, Pt particles were the main components of the PtSn-C and PtSn-B-HCl series (Figure 3d,f,h). After hydrogen reduction of the PtSn-B-HCl series, the characteristic peaks of Pt disappeared, suggesting that Pt may be effectively dispersed, with a reduction of the particle size. Notably, the peaks of the Pt<sub>3</sub>Sn alloy appeared after hydrogen reduction of the PtSn-B-HCl series (Figure 3g,i). In terms of the Pt-Sn alloys, the PtSn alloy having a Pt/Sn molar ratio of 1:1 is often referred to; however, it is known that various forms, such as PtSn, Pt<sub>3</sub>Sn, and Pt<sub>2</sub>Sn<sub>3</sub>, are possible [39–43]. Vu et al. [44] presented the characteristic XRD peaks of the Pt<sub>3</sub>Sn alloy and Sattler et al. [45] also verified the existence of the Pt<sub>3</sub>Sn alloy using TEM measurement. Both cases utilized propane feedstock. The reaction atmosphere may affect the formation of the Pt-Sn alloys. Herein, a mixture of propane, hydrogen, and nitrogen was used.

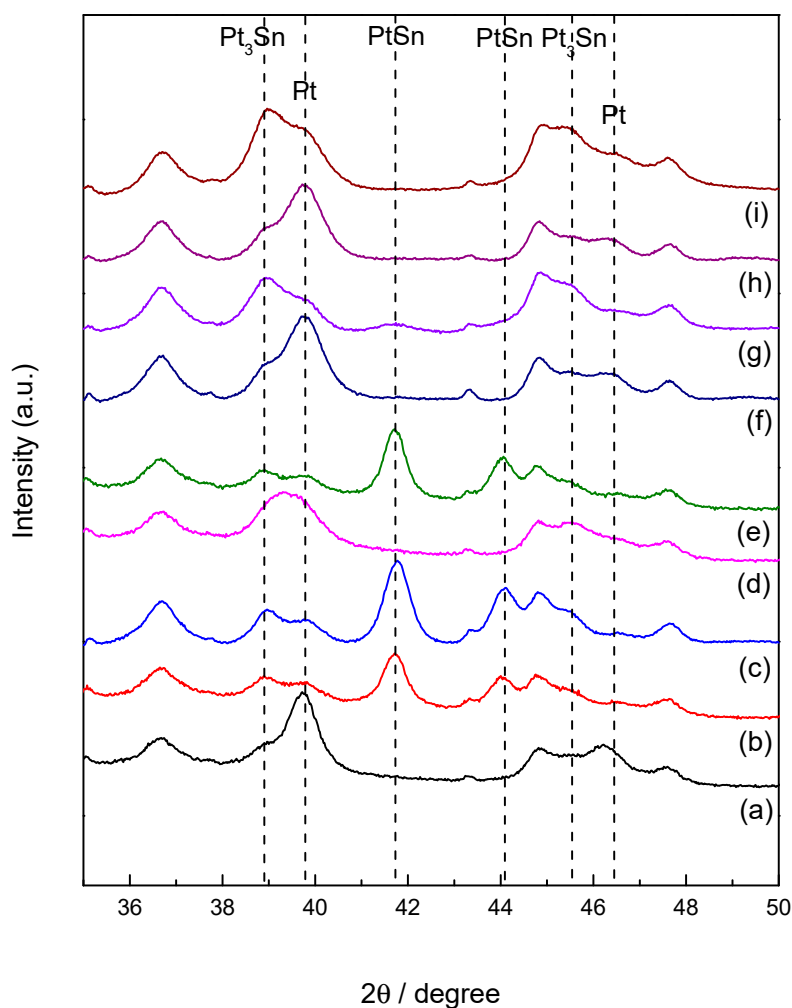


**Figure 3.** X-ray diffraction (XRD) patterns of Pt-Sn/Al<sub>2</sub>O<sub>3</sub> catalysts after catalyst preparation: (a) PtSn-C, (b) reduced PtSn-C, (c) PtSn-U, (d) PtSn-B, (e) reduced PtSn-B, (f) PtSn-B-HCl5, (g) reduced PtSn-B-HCl5, (h) PtSn-HCl35, and (i) reduced PtSn-B-HCl35.

### 2.2.2. TEM and EDS

EDX images and TEM images of catalysts are shown in Figures 4 and 5, respectively. The dispersion and the sizes of the metal particles before and after the regeneration treatments were compared. The particle size of the metals increased after coke burning (PtSn-B). HCl treatment effectively reduced the size of the metal particles in the catalysts, regardless of the HCl concentration. Better dispersity of the metal particles was observed in PtSn-B-HCl35. More details were derived from FFT analysis. The TEM images (the inset shows the corresponding FFT pattern) in Figure 6 were employed to calculate the lattice distance in the crystals. The existence of both the PtSn alloy and Pt<sub>3</sub>Sn alloy was also verified. The lattice distance data were compared by calculation of the PDF and by comparison with the ICDD cards. The FFT image of PtSn-B after hydrogen reduction was used to derive the lattice distance data for the four faces of the PtSn alloy. The lattice distances were 0.22, 0.3, 0.36, and 0.17 nm for the (102), (101), (100), and (201) planes, respectively. The FFT image of PtSn-B-HCl35 after reduction indicated the presence of both the PtSn alloy and Pt<sub>3</sub>Sn alloy. In the PtSn alloy, the lattice distance of the (100) plane was 0.3 nm. In the case of the Pt<sub>3</sub>Sn alloy, the lattice distances were 0.12, 0.18, and 0.23 nm for the (311), (111), and (210) planes, respectively. The FFT image of PtSn-B-HCl5 after reduction also indicated the existence of both the PtSn and Pt<sub>3</sub>Sn alloy. The lattice distances for the PtSn alloy were 0.3 and 0.2 nm for the (101) and (110) planes, respectively. The lattice distance was 0.28 nm for the (110) plane of the Pt<sub>3</sub>Sn alloy. It was verified that the redispersion of Pt was achieved by HCl treatment.

Notably, HCl treatment induced the formation of the Pt<sub>3</sub>Sn alloy, which resulted in higher catalytic activity. Treatment with 35% HCl (PtSn-B-HCl35) was the most effective for metal dispersion and enhancing the catalyst activity.

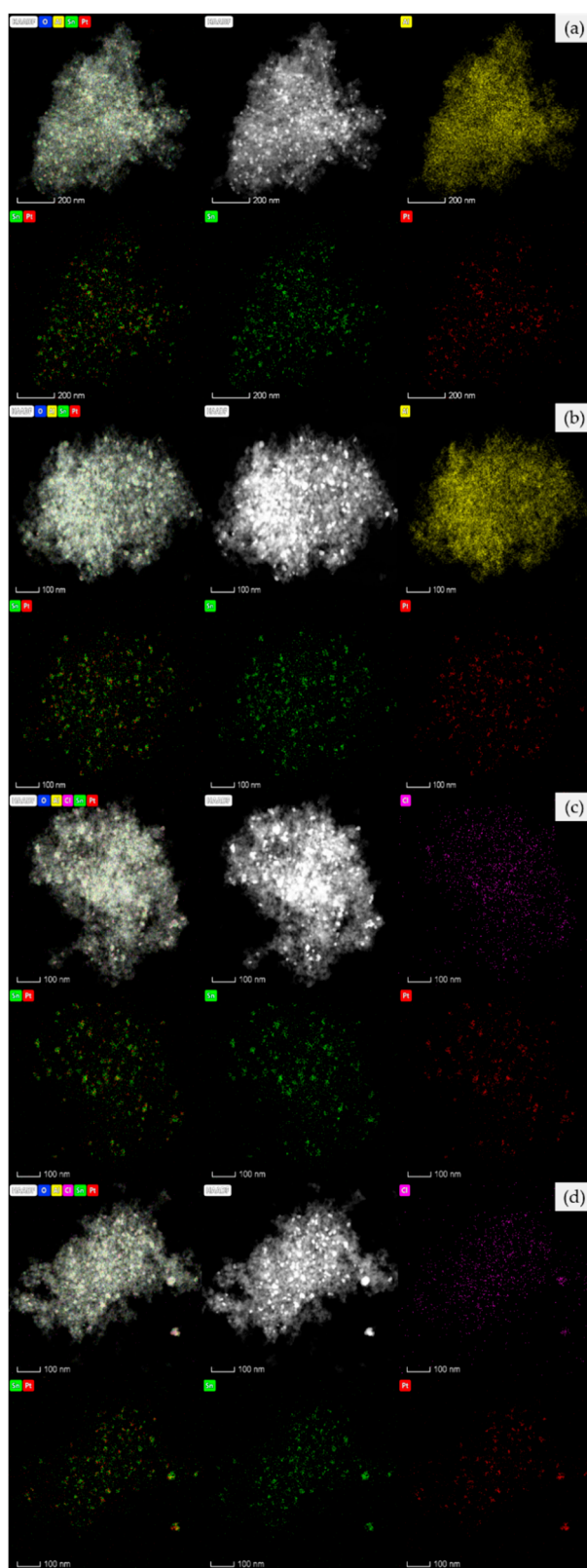


**Figure 4.** Energy dispersive X-ray (EDX) element mapping images of (a) reduced PtSn-C, (b) reduced PtSn-B, (c) reduced PtSn-B-HCl5, and (d) reduced PtSn-B-HCl35.

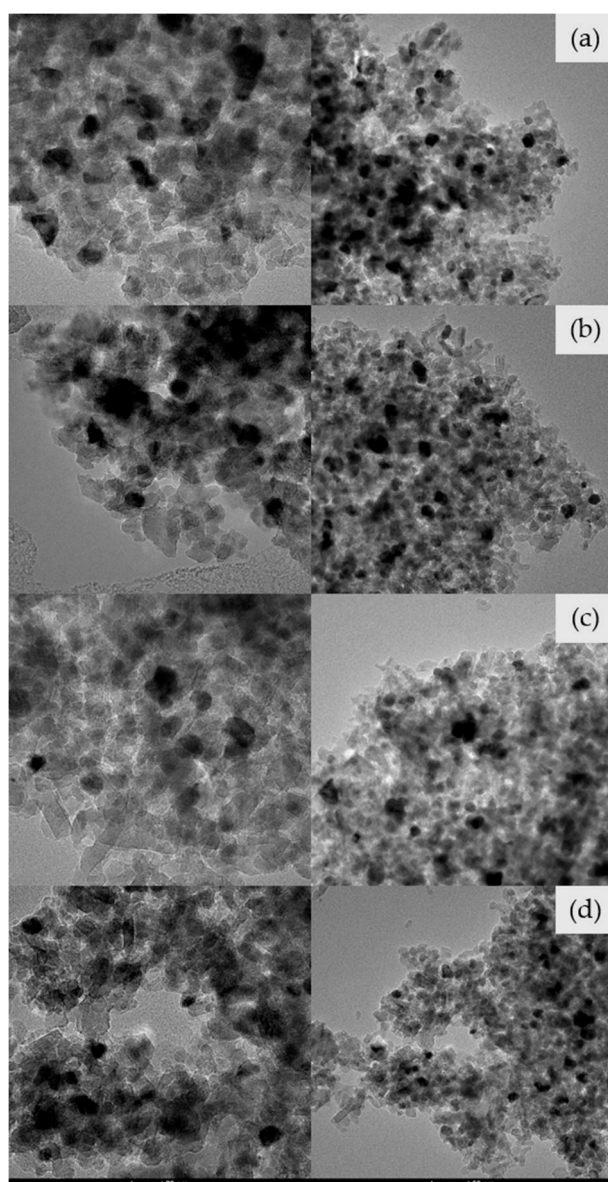


**Figure 5.** Transmission electron microscopy (TEM) images of (a) reduced PtSn-C, (b) reduced PtSn-B, (c) reduced PtSn-B-HCl5, and (d) reduced PtSn-B-HCl35.

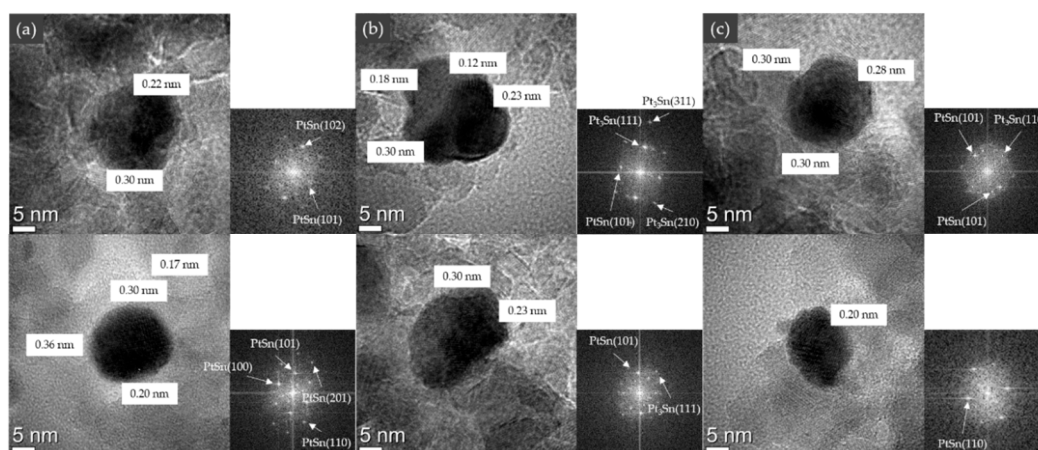


**Figure 6.** TEM images (inset shows the corresponding FFT pattern) of (a) reduced PtSn-B, (b) reduced PtSn-B-HCl5, and (c) reduced PtSn-B-HCl35.

### 2.2.3. XPS Analysis

Four catalysts of the PtSn-B-HCl series were subjected to XPS measurement. All catalysts were recorded at Pt 4f (Figure 7) and Sn 3d (Figure 8). As there are overlapping ranges of characteristic peaks between Pt 4f and Al 2P [46], we focused on Pt 4d in this work. Thus, we focus on the Pt 4d region in this work. Other previous works were adapted to analyze the Pt 4f data [47,48]. Evidence of the Pt state was provided by the Pt  $4d_{5/2}$  peak at 315.2 eV in Figure 7. Figure 8 compares the effect of the HCl concentration on the catalysts. The peaks did not change significantly with variation of the HCl concentration. It was reported that the characteristic peaks of  $\text{Sn}^0$  appear in the range of 485.2–486.5 eV, and the characteristic peaks of  $\text{Sn}^{2+}/\text{Sn}^{4+}$  appear at 487.2–488.3 eV. Peaks were observed in both characteristic ranges at 485.5 and 487.2~488.3 eV, respectively, which indicates the existence of  $\text{Sn}^0$  and  $\text{Sn}^{2+}/\text{Sn}^{4+}$ . It is difficult to differentiate  $\text{Sn}^{2+}$  and  $\text{Sn}^{4+}$  because the peaks of both species are extremely close, as reported earlier [47,49]. Figure 8 presents the changes in the Sn  $3d_{5/2}$  peak with respect to the HCl concentration used during the regeneration process. All catalysts of the PtSn-B-HCl series showed peaks of  $\text{Sn}^0$  and  $\text{Sn}^{2+}/\text{Sn}^{4+}$ . Before reduction of PtSn-C, the characteristic peak of  $\text{Sn}^0$  was relatively weak, but the intensity clearly increased after reduction. In the case of the PtSn-B-HCl series, the characteristic peaks of  $\text{Sn}^0$  were also intensified after reduction of the catalyst.

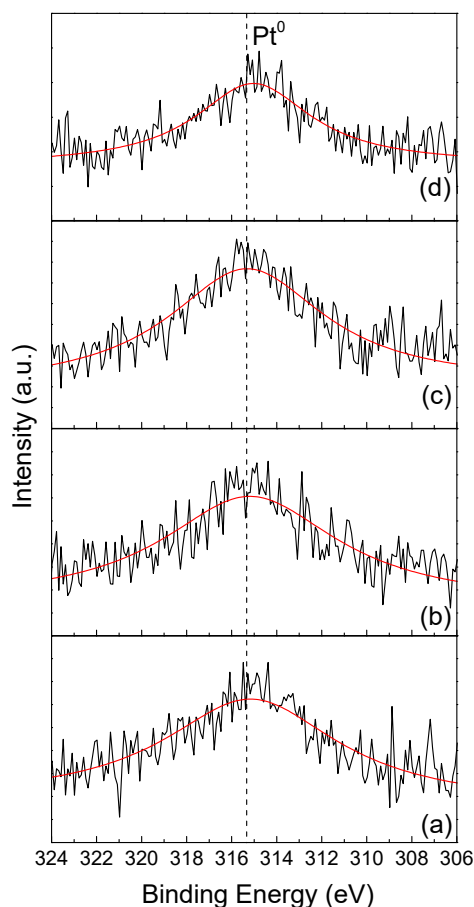


**Figure 7.** X-ray photoelectron spectroscopy (XPS) Pt 4f curves of catalysts. (a) PtSn-C, (b) PtSn-B, (c) PtSn-B-HCl5, and (d) PtSn-B-HCl35.

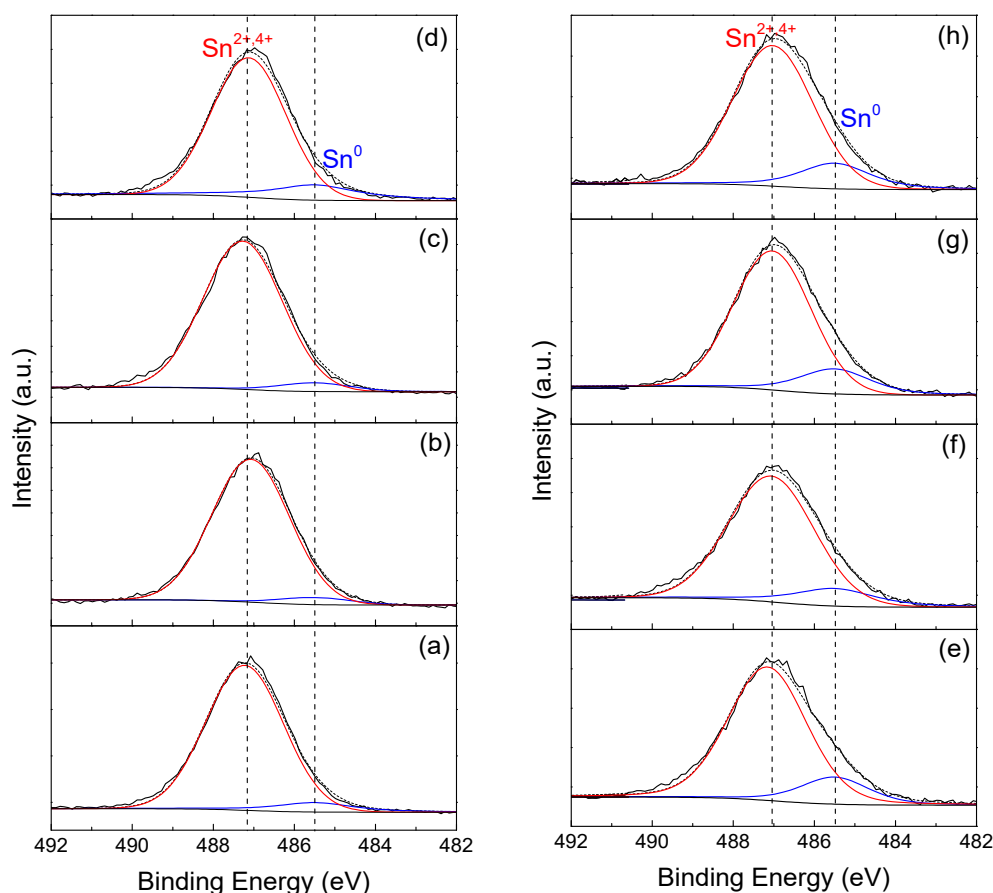


**Figure 8.** XPS Sn 3d curves of catalysts. (a) PtSn-C, (b) PtSn-B, (c) PtSn-B-HCl5, (d) PtSn-B-HCl35, (e) reduced PtSn-C, (f) reduced PtSn-B, (g) reduced PtSn-B-HCl5, and (h) reduced PtSn-B-HCl35.

#### 2.2.4. TPR Analysis

TPR analysis was performed to examine the interaction between the catalyst support and metal particles. Two peaks were noticeable for PtSn-C at 330 °C (weak) and 400 °C (strong). The TPR profiles of all catalysts showed two peaks, presenting evidence of reduction. In the case of the regenerated catalysts, the two peaks at 330 °C and 400 °C almost disappeared, while two new peaks appeared in the ranges of 280–330 °C and 480–530 °C. Under the various regeneration conditions, the peak at 330 °C for PtSn-C shifted to the lower temperature range of 280–330 °C and the peak became more intense. The peaks at 280–330 °C for the three catalysts were attributed to Pt oxides. In general, the characteristic TPR peak of the Pt particles appeared at 200 °C or lower. The peak shift to 280–330 °C, that is, higher than 200 °C, was presumed to be owing to Sn addition. The first peak was observed at 330, 283, 297, and 323 °C for PtSn-C, PtSn-B, PtSn-B-HCl5, and PtSn-B-HCl35, respectively. Notably, the first peak of PtSn-C and PtSn-B-HCl35 occurred at very close temperatures, which implies that similar catalytic activity can be expected for PtSn-C and PtSn-B-HCl35. When PtSn-C was initially prepared, the average distance between Pt and Sn appeared to be relatively small because of the impregnation method used in this work. In the case of PtSn-B, the TPR curves showed that the overall interactions between Pt and Sn became less. This may be because Pt sintering was accelerated during coke burning. Returning to Figure 3d, Sn present in the PtSn alloy may be expelled to form Sn oxides, leaving more individual Pt from the PtSn alloy phase. If subsequent HCl treatment is performed, the behaviors of Pt and Sn will be altered. In the case of Sn, HCl treatment may dissolve Sn/SnO<sub>x</sub> located on the surfaces of the Pt particles and/or alumina support, and in the edges between Pt and the alumina support. Consequently, HCl treatment could force Sn/SnO<sub>x</sub> to migrate some distance from the Pt-occupied sites. Quantitatively, the majority of Sn may stay on the surface of the alumina support and little may be

localized on either the edges near the Pt particle or on the surface of the Pt particles. That is, little, but relatively well-dispersed Sn/SnO<sub>x</sub> can sit on the surface of the Pt particles, which may provide an advantageous environment for generating the Pt<sub>3</sub>Sn alloy rather than the PtSn alloy during the calcination step of the HCl treatment. (See Figure 9).

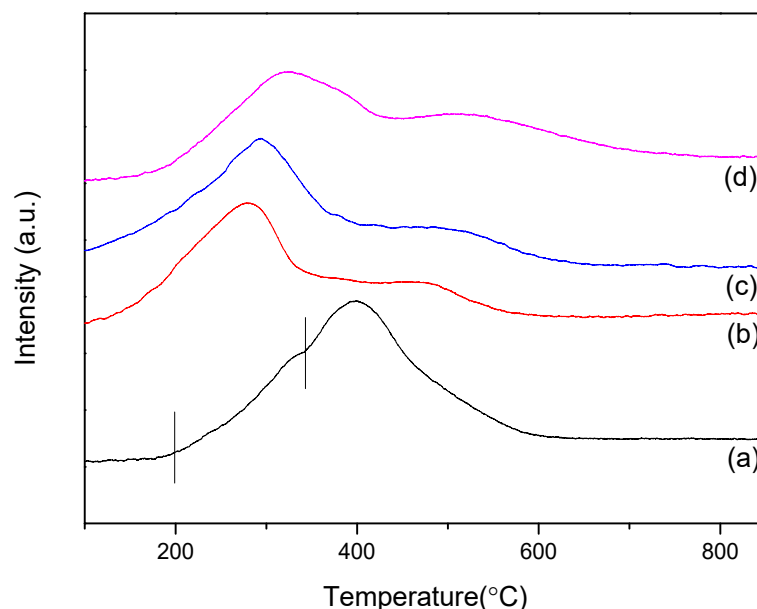


**Figure 9.** Temperature-programmed reduction (TPR) curves of catalysts. (a) PtSn-C, (b) PtSn-B, (c) PtSn-B-HCl5, and (d) PtSn-B-HCl35.

### 2.2.5. CO Chemisorption

Table 2 presents the CO chemisorption data for the Pt-Sn catalysts, along with the metal dispersion, metal surface area, average particle size, and coke content. The data for PtSn-C is presented as a reference. The metal dispersion, surface area, and average particle size of PtSn-C were 4.63%, 0.34 m<sup>2</sup>/g-cat, and 24.45 nm, respectively. The metal dispersion of PtSn-B decreased from 4.63 to 4.03. A lower HCl concentration (5%) was not effective for increasing the metal dispersion. Higher than 15% of HCl led to improved metal dispersion, with much higher values (5.08–7.09%) than that of PtSn-C (4.63%). The metal surface area and average particle size followed similar trends. The metal surface area and average particle size of PtSn-B and PtSn-B-HCl5 were undesirably smaller and larger, respectively, than those of PtSn-C in. In the PtSn-B-HCl series, PtSn-B-HCl35 had the highest metal surface area (0.53 m<sup>2</sup>/g-cat) and smallest average particle size (15.98 nm). The coke content is presented to compare the effect of the regeneration process. Various coke types were formed during the PDH reaction and were quantified separately. Compared with 3.24% coke in PtSn-B, the coke formation was reduced to 3.03% in PtSn-B-HCl35.

**Table 2.** CO chemisorption data for catalysts.

| Catalyst     | Amount of CO Adsorbed (cm <sup>3</sup> STP g <sup>-1</sup> cat) | Metal Dispersion (%) | Metal Surface Area (m <sup>2</sup> g <sup>-1</sup> cat) | Average Particle Size (nm) | Coke Content <sup>a</sup> (wt%) |
|--------------|---|----------------------|---|----------------------------|---------------------------------|
| PtSn-C       | 0.16  | 4.63                 | 0.34  | 24.45                      | -                               |
| PtSn-B       | 0.14  | 4.03                 | 0.30  | 28.10                      | 3.24                            |
| PtSn-B-HCl5  | 0.09  | 2.57                 | 0.19  | 43.66                      | -                               |
| PtSn-B-HCl15 | 0.24  | 6.85                 | 0.51  | 16.55                      | 4.24                            |
| PtSn-B-HCl25 | 0.18  | 5.08                 | 0.38  | 22.29                      | 2.93                            |
| PtSn-B-HCl35 | 0.24  | 7.09                 | 0.53  | 15.98                      | 3.03                            |

<sup>a</sup> coke amount was determined by thermal gravitational analysis.

### 3. Discussion

The results show that two major factors affect the generation of the Pt<sub>3</sub>Sn alloy during the regeneration process. One is the initial molar ratio between Pt and Sn during catalyst preparation. The other is the specific treatment for regeneration, such as the oxychlorination process. In our previous study [32], the Pt/Sn ratio of was set to 1 to 0.5 by weight, which corresponds to a Pt/Sn molar ratio of 1.23 to 1. When the fresh catalyst was prepared, there was no evidence of the Pt<sub>3</sub>Sn alloy. After the first run of PDH, no Pt<sub>3</sub>Sn alloy was detected, even after coke burning. Coke burning was used as the primary process for regeneration of the Pt-Sn catalyst, followed by oxychlorination treatment as a second process. HCl and air were fed into the reactor at a high temperature of 550 °C [32], after which the Pt<sub>3</sub>Sn alloy was detected by XRD. Thus, generation of the Pt<sub>3</sub>Sn alloy was triggered by the secondary oxychlorination treatment. Another study used the molar ratio of 1 to 1 for Pt to Sn [50]. In that case, direct reduction was employed and the Pt<sub>3</sub>Sn alloy was detected in the fresh catalysts. Direct reduction was attempted before the first run of PDH in that case. In this work, the Pt/Sn ratio was set to 3 to 4.5 by weight, which is close to the Pt/Sn molar ratio of 1 to 2.5. If the molar ratio of Pt/Sn is less than 1, the Pt<sub>3</sub>Sn alloy is hardly formed, whereas formation of the PtSn alloy is favored. As expected, the Pt<sub>3</sub>Sn alloy was not detected in the fresh catalyst, even after coke burning. However, the Pt<sub>3</sub>Sn alloy was formed after HCl treatment. The present HCl treatment includes immersion, drying, and calcination, which is analogous to our prior oxychlorination treatment [32]. It seems that calcination plays a role similar to oxychlorination in dispersing the Pt particles as well as generating the Pt<sub>3</sub>Sn alloy. As mentioned above, the initial Pt/Sn weight ratio was controlled to 3 to 4.5, which appears to favor formation of the PtSn alloy than Pt<sub>3</sub>Sn in the initial condition. During HCl treatment, the interactions between Pt and HCl and between Sn/SnO<sub>x</sub> and HCl may contribute differently to forming the Pt-Sn alloys. If concentrated liquid HCl easily dissolves and migrates Sn/SnO<sub>x</sub> constituents far from the sites nearby Pt, the interfaces between Pt and Sn/SnO<sub>x</sub> may change to lower, but more well-dispersed SnO<sub>x</sub> on the surface of Pt particles. If this happens, a lesser amount of wished-off Sn/SnO<sub>x</sub> can be placed on the surface of Pt particles, where we defined the Pt-rich phase. If Pt particles in the Pt-rich phase may redisperse during calcination for HCl treatment, Pt<sub>3</sub>Sn alloy is more favorably generated than PtSn alloy. This is different with the case after coke burning only. That is, when coke burning proceeds, Pt and Sn/SnO<sub>x</sub> could not migrate too far from original locations. If this is true, PtSn alloy is more favorable to form than Pt<sub>3</sub>Sn alloy during coke burning.

### 4. Materials and Methods

#### 4.1. Catalyst Preparation

The overall procedure for preparing Pt-Sn/Al<sub>2</sub>O<sub>3</sub> is similar to the method published earlier [50]. Aluminum-oxide-supported Pt-Sn catalysts were prepared with 3 wt.% Pt and 4.5 wt.% Sn using hydrogen hexachloroplatinate(IV) hydrate (H<sub>2</sub>PtCl<sub>6</sub>·6H<sub>2</sub>O, Kojima Chemicals, Saitama, Japan) and tin(II) chloride (SnCl<sub>2</sub>, Sigma-Aldrich, St. Louis, MO, USA, >98%) through a co-impregnation method using ethanol (C<sub>2</sub>H<sub>5</sub>OH, 99.5%, Daejung, Seoul, Korea). The catalysts were dried at 110 °C for 12 h under air atmosphere in an oven and then calcined at 600 °C for 4 h at a heating rate of 5 °C min<sup>-1</sup>.

#### 4.2. Catalytic Activity Measurements

The work scope of this study is presented in Figure 10. The catalytic activity during the PDH reaction was evaluated in a fixed-bed quartz reactor (inner diameter of 18 mm) using 0.3 g of catalyst. The PDH reaction was carried out at 600 °C for 3 h at atmospheric pressure in the presence of C<sub>3</sub>H<sub>8</sub> (30 mL min<sup>-1</sup>), H<sub>2</sub> (30 mL min<sup>-1</sup>), and N<sub>2</sub> (70 mL min<sup>-1</sup>). Before the PDH reaction, the samples were heated to 600 °C at 10 °C min<sup>-1</sup> in the presence of H<sub>2</sub> (30 mL min<sup>-1</sup>) and N<sub>2</sub> (100 mL min<sup>-1</sup>). After the PDH reaction, coke burning was carried out under air atmosphere at 510 °C for 4 h. Hydrochloric acid (HCl) treatment was performed using four different concentrations: 5, 15, 25, and 35% by weight. After HCl treatment, the catalyst was dried at 110 °C for 12 h and calcined at 600 °C for 4 h. These amplex

are denoted as PtSn-B-HCl5, PtSn-B-HCl15, PtSn-B-HCl25, and PtSn-B-HCl35, respectively. Hydrogen reduction was additionally performed at 600 °C for 1 h. The second PDH reaction was carried out at 600 °C for 3 h. WHSV of two reaction test set is 11.8 h<sup>-1</sup>.

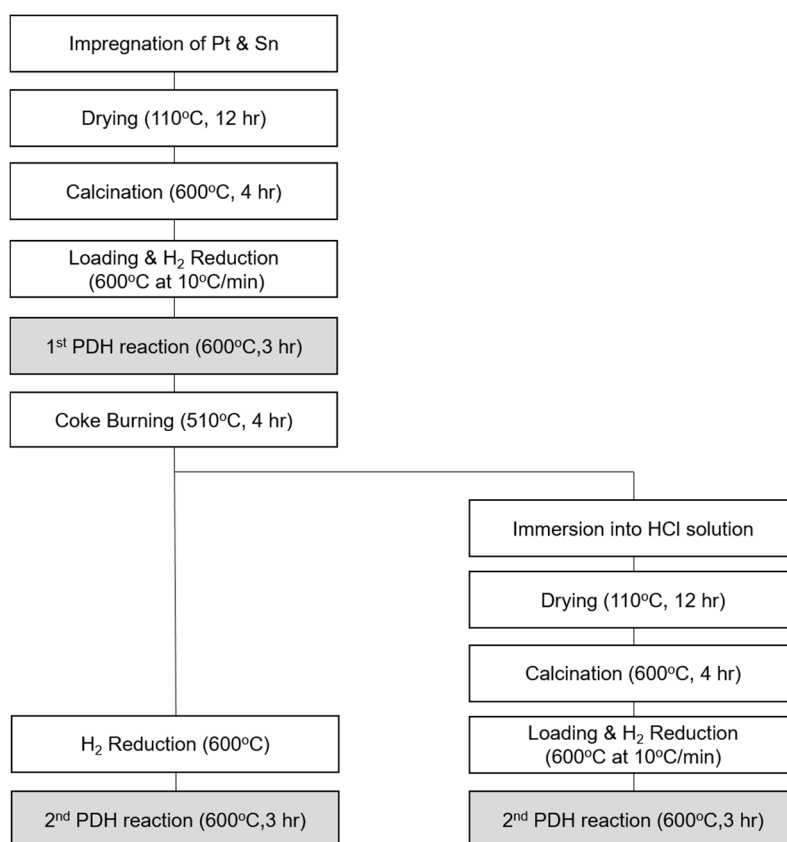


**Figure 10.** Diagram of the work scope of this study.

The product gases were analyzed using a gas chromatography apparatus (flame ionization detector, 5890 Series 2 Plus, Hewlett Packard, Wilmington, DE, USA) equipped with a capillary column (GS-Alumina, Agilent Technologies, Santa clara, CA, USA, inner diameter: 0.53 mm, length: 50 m). The propane conversion, propylene selectivity, and propylene yield were calculated using the following equations:

$$\text{Propane conversion (\%)} = 1 - \frac{[\text{CH}_4] + 2[\text{C}_2\text{H}_4] + 2[\text{C}_2\text{H}_6] + 3[\text{C}_3\text{H}_6]}{[\text{CH}_4] + 2[\text{C}_2\text{H}_4] + 2[\text{C}_2\text{H}_6] + 3[\text{C}_3\text{H}_6] + 3[\text{C}_3\text{H}_8]} \times 100$$

$$\text{Propylene selectivity (\%)} = \frac{3[\text{C}_3\text{H}_6]}{[\text{CH}_4] + 2[\text{C}_2\text{H}_4] + 2[\text{C}_2\text{H}_6] + 3[\text{C}_3\text{H}_6]} \times 100$$

$$\text{Propylene yield (\%)} = \frac{\text{Propane Conversion} \times \text{Propylene Selectivity}}{100}$$

where [C<sub>3</sub>H<sub>8</sub>], [C<sub>3</sub>H<sub>6</sub>], [C<sub>2</sub>H<sub>6</sub>], [C<sub>2</sub>H<sub>4</sub>], and [CH<sub>4</sub>] refer to the concentration of outlet gas component. Conversion recovery and selectivity recovery were calculated by equations as follows:

$$\text{Conversion recovery (\%)} = \frac{\text{Propane conversion in 2nd PDH reaction after regeneration}}{\text{Propane conversion in 1st PDH reaction}} \times 100$$

$$\text{Selectivity recovery (\%)} = \frac{\text{Propylene selectivity in 2nd PDH reaction after regeneration}}{\text{Propylene selectivity in 1st PDH reaction}} \times 100$$

### 4.3. Characterization

The crystalline phases of Pt-Sn/Al<sub>2</sub>O<sub>3</sub> and regenerated Pt-Sn/Al<sub>2</sub>O<sub>3</sub> were examined using XRD (D'Max 2500/PC, Rigaku, Tokyo, Japan). The operating voltage and current were 40 kV and 200 mA, respectively. Scanning was performed in the 2θ range 20°–90°, at a scanning rate of 4° min<sup>-1</sup>. TEM images were obtained using FEI Tecnai G2-20 S-Twin and FEI Titan<sup>TM</sup> 80–300 instruments (Hillsboro, OR, USA) operating at an accelerating voltage of 200 kV. TEM mapping images were obtained using an FEI transmission electron microscope (Hillsboro, OR, USA). The metal dispersion was measured by CO chemisorption using a Micromeritics ASAP2020 volumetric analyzer (Norcross, GA, USA). A fixed amount of each catalyst (0.5 g) was treated under He gas flow at 110 °C for 0.5 h. Subsequently, the pretreated catalysts were heated from room temperature to 350 °C under pure H<sub>2</sub> flow for 3 h. In the subsequent reduction, a purge step was performed under He gas flow at the same temperature for 2 h. The sample was cooled to 35 °C and purged under He gas flow for 2 h. After pretreatment, the catalyst was subjected to a flow of CO as an adsorbate for total adsorption measurements. Afterward, the catalyst was evacuated to remove the physically adsorbed CO, and the CO flow was initiated again for the physical adsorption measurements. The amount of chemisorbed CO was determined by analyzing the difference between the two quantities of adsorbed CO. To analyze the chemical states of the elements, XPS spectra were obtained with a PHI 5000 Versa Probe spectrometer (Ulvac-PHI) equipped with a monochromatic electroanalyzer (Kanagawa, Japan) and a monochromatic Al-Kα 150 W X-ray source.

Temperature-programmed reduction (TPR) was used to measure the reducibility of the catalysts using a Micromeritics Auto-Chem II 2910 apparatus (Norcross, GA, USA). The samples (0.1 g) were loaded into the quartz reactor. Prior to TPR analysis, the samples were dried under flowing N<sub>2</sub> at 500 °C for 1 h (30 mL min<sup>-1</sup>). The TPR profiles were then recorded under 10% H<sub>2</sub>/Ar flow in the temperature range of 50–900 °C at a heating rate of 10 °C min<sup>-1</sup>. The hydrogen consumption was continuously monitored as a function of the reduction temperature by a TCD cell and recorded. The amount of coke after the propane dehydrogenation of the spent catalysts was determined by thermogravimetric analyzer (SDT Q600, TA Instruments, New Castle, DE, USA) from room temperature to 850 °C at 5 °C min<sup>-1</sup> under flowing air (100 mL min<sup>-1</sup>).

## 5. Conclusions

Pt-Sn catalysts are widely used in PDH. Coke generation during PDH is inevitable, and the generated coke must be removed from the catalyst periodically. Coke burning is a typical option for catalyst regeneration. However, coke burning results in extensive Pt sintering. In order to maintain the catalyst activity, an extended treatment was explored for redispersing the metal catalysts. In our prior work, oxychlorination treatment after coke burning was attempted, and enhanced the performance in successive PDH runs. In this work, Pt-Sn/Al<sub>2</sub>O<sub>3</sub> catalysts were regenerated by treatment with liquid hydrochloric acid after coke burning. Here, the protocol of HCl treatment includes three stages: immersion of the catalysts in liquid HCl solution, drying, and calcination. The results suggest that the current HCl treatment may be effective for regenerating Pt-Sn catalysts supported on alumina. The Pt and Sn loadings used in the fresh catalyst were 3 and 4.5% by weight (PtSn-C). For clear comparison, we coined two new terms: the conversion recovery and the selectivity recovery. The conversion and selectivity recovery were calculated as the ratio of the propane conversion and propylene selectivity, respectively, for the first PDH run versus the second PDH run. Propane conversion recovery was achieved by HCl treatment. This study focuses on evaluating the effectiveness of HCl treatment after coke burning. The catalysts subjected to HCl treatment were termed the PtSn-B-HCl series. The effect

of different HCl concentrations (5–35% *w/w* in water) was examined, where the HCl-treated catalysts are termed PtSn-B-HCl5 to PtSn-B-HCl35. The optimal conversion recovery was achieved by treatment with 35% HCl (PtSn-B-HCl35). The improved catalyst activity is attributed to two factors: effective redispersion of the Pt particles and formation of the Pt<sub>3</sub>Sn alloy. HCl treatment acted analogously to oxychlorination treatment. It seems that the calcination during HCl treatment played a similar role as oxychlorination in dispersing the Pt particles as well as generating the Pt<sub>3</sub>Sn alloy. As mentioned above, the initial ratios of Pt and Sn were controlled to 3 to 4.5, which is more favorable for forming the PtSn alloy rather than Pt<sub>3</sub>Sn during hydrogen reduction. With the addition of hydrochloric acid, the interactions between Pt and HCl and between Sn/SnO<sub>x</sub> and HCl may contribute differently to inducing the formation of different Pt-Sn alloys. If Sn/SnO<sub>x</sub> is easily dissolved in HCl and migrates away from the Pt sites, the interfaces between Pt and Sn/SnO<sub>x</sub> change to less, but well-dispersed SnO<sub>x</sub> on the surface of the Pt particles, which we defined as a Pt-rich phase. If the Pt particles in the Pt-rich phase are effectively redispersed during calcination for HCl treatment, the Pt<sub>3</sub>Sn alloy is more favorably generated than the PtSn alloy. This is different from the case after plain coke burning. In other words, during coke burning, Pt and Sn/SnO<sub>x</sub> cannot migrate too far from the original sites. In such a case, the PtSn alloy is generated in preference to the Pt<sub>3</sub>Sn alloy after the ensuing reduction. Because more SnO<sub>x</sub> covers the surface of the Pt particles, where the ratio of Pt to Sn may be larger than 1, the PtSn alloy is favorably formed during the ensuing reduction process. In addition, redispersion of the metals was examined by TPR. Both coke burning and HCl treatment led to separation of the Pt and SnO<sub>x</sub> phases. However, after HCl treatment, the degree of separation between the Pt and SnO<sub>x</sub> phases was recovered to the initial condition. The improved redispersion was also verified by CO chemisorption. The metal dispersion, metal surface area, and average particle size were all improved for PtSn-B-HCl35 after HCl treatment compared with the plain coke burning process. HCl treatment may be applicable to the regeneration of catalysts in PDH plants. In industrial PDH operation, chlorine gas or CCl<sub>4</sub> can be added to regenerate Pt-Sn catalyst after coke burning. If the concept of this study works, we can expect to use concentrated HCl for alternative treatment to current chlorine-based oxychlorination options.

**Author Contributions:** The experimental work was designed and performed by Y.S.C.; K.-D.J. and W.-I.K. analyzed the data; writing, review, and editing were done by K.O.; writing and original draft preparation were done by H.L.K. All authors have read and agreed to the published version of the manuscript.

**Funding:** This work was financed by the Basic Science Research Program through the National Research Foundation of Korea (NRF) funded by the Ministry of Education (2017R1D1A1B03034244).

**Conflicts of Interest:** The authors declare no conflicts of interest.

## References

1. Wannapakdee, W.; Yutthalekha, T.; Dugkhuntod, P.; Rodponthukwaji, K.; Thivasasith, A.; Nokbin, S.; Witoon, T.; Pengpanich, S.; Wattanakit, C. Dehydrogenation of propane to propylene using promoter-free hierarchical Pt/Silicalite-1 nanosheets. *Catalysts* **2019**, *9*, 174. [[CrossRef](#)]
2. Tolek, W.; Suriye, K.; Praserthdam, P.; Panpranot, J. Effect of preparation method on the Pt-In modified Mg(Al)O catalysts over dehydrogenation of propane. *Catal. Today* **2019**, in press. [[CrossRef](#)]
3. Searles, K.; Chan, K.W.; Burak, J.A.M.; Zemlyanow, D.; Safonova, O.; Copéret, C. Highly productive propane dehydrogenation catalyst using silica supported Ga-Pt nanoparticles generated from single-sites. *J. Am. Chem. Soc.* **2018**, *140*, 11674–11679. [[CrossRef](#)] [[PubMed](#)]
4. Shenjun, Z.; Guodong, S.; Tengfang, W.; Jiubing, Z.; Zhi-Jian, Z.; Jinlong, G. Identification of Pt-based catalysts for propane dehydrogenation via a probability analysis. *Chem. Sci.* **2018**, *9*, 3925–3931.
5. NaKaYa, Y.; Hirayama, J.; Yamazoe, S.; Shimizu, K.; Furukawa, S. Single-atom Pt in intermetallics as an ultrastable and selective catalyst for propane dehydrogenation. *Nat. Commun.* **2020**, *11*, 2838–2844. [[CrossRef](#)] [[PubMed](#)]
6. Ge, M.; Chen, X.; Li, Y.; Wang, J.; Xu, Y.; Zhang, L. Perovskite-derived cobalt-based catalyst for catalytic propane dehydrogenation. *React. Kinet. Mech. Catal.* **2020**, *130*, 241–256. [[CrossRef](#)]

7. Sricharoen, C.; Jongsomjit, B.; Panpranot, J.; Praserttham, P. The key to catalytic stability on sol-gel derived SnO<sub>x</sub>/SiO<sub>2</sub> catalyst and the comparative study of side reaction with K-PtSn/Al<sub>2</sub>O<sub>3</sub> toward propane dehydrogenation. *Catal. Today* **2020**, in press. [[CrossRef](#)]
8. Ji, Z.; Miao, D.; Gao, L.; Pan, X.; Bao, X. Effect of pH on the catalytic performance of PtSn/B-ZrO<sub>2</sub> in propane dehydrogenation. *Chin. J. Catal.* **2020**, *41*, 719–729. [[CrossRef](#)]
9. Liu, Q.; Luo, M.; Zhao, Z.; Zhao, Q. K-modified Sn-containing dendritic mesoporous silica nanoparticles with tunable size and SnO<sub>x</sub>-silica interaction for the dehydrogenation of propane to propylene. *Chem. Eng. J.* **2020**, *380*, 122423–122434.
10. An-Hua, D.; Kang, W.; Shi-Zhen, Z.; Gong-Bing, Y.; Xi-Tao, W. Facile preparation of PtSn-La/Al<sub>2</sub>O<sub>3</sub> catalyst with large pore size and its improved catalytic performance for isobutane dehydrogenation. *Fuel Process. Technol.* **2017**, *158*, 218–225.
11. Pham, H.N.; Sattler, J.J.H.B.; Weckhuysen, B.M.; Datye, A.K. Role of Sn in the regeneration of Pt/γ-Al<sub>2</sub>O<sub>3</sub> light alkane dehydrogenation catalysts. *ACS Catal.* **2016**, *6*, 2257–2264. [[CrossRef](#)] [[PubMed](#)]
12. Chen, X.; Ge, M.; Li, Y.; Liu, Y.; Wang, J.; Zhang, L. Fabrication of highly dispersed Pt-based catalysts on γ-Al<sub>2</sub>O<sub>3</sub> supported perovskite Nano islands: High durability and tolerance to coke deposition in propane dehydrogenation. *Appl. Surf. Sci.* **2019**, *490*, 611–621. [[CrossRef](#)]
13. Cybulskis, V.J.; Bukowski, B.B.; Tseng, H.; Gallagher, J.R.; Wu, Z.; Wegener, E.; Kropf, A.J.; Ravel, B.; Ribeiro, F.H.; Greeley, J.; et al. Zinc promotion of platinum for catalytic light alkane dehydrogenation: Insights into geometric and electronic effects. *ACS Catal.* **2017**, *7*, 4173–4181. [[CrossRef](#)]
14. Kaylor, N.; Davis, R.J. Propane dehydrogenation over supported Pt-Sn nanoparticles. *J. Catal.* **2018**, *367*, 181–193. [[CrossRef](#)]
15. Liu, J.; Li, J.; Rong, J.; Liu, C.; Dai, Z.; Bao, J.; Da, Z.; Zheng, H. Defect-driven unique stability of Pt/carbon nanotubes for propane dehydrogenation. *Appl. Surf. Sci.* **2019**, *464*, 146–152. [[CrossRef](#)]
16. Wang, G.; Zhang, H.; Zhu, Q.; Zhu, X.; Li, X.; Wang, H.; Li, C.; Shan, H. Sn-containing hexagonal mesoporous silica (HMS) for catalytic dehydrogenation of propane: An efficient strategy to enhance stability. *J. Catal.* **2017**, *351*, 90–94. [[CrossRef](#)]
17. Srisakwattana, T.; Suriye, K.; Praserttham, P.; Panpranot, J. Preparation of aluminum magnesium oxide by different methods for use as PtSn catalyst supports in propane dehydrogenation. *Catal. Today* **2019**, in press. [[CrossRef](#)]
18. Long, L.; Xia, K.; Lang, W.; Shen, L.; Yang, Q.; Yan, X.; Guo, Y. The comparison and optimization of zirconia, alumina, and zirconia-alumina supported PtSnIn trimetallic catalysts for propane dehydrogenation reaction. *J. Ind. Eng. Chem.* **2017**, *51*, 271–280. [[CrossRef](#)]
19. Zhou, H.; Gong, J.; Xu, B.; Deng, S.; Ding, Y.; Yu, L.; Fan, Y. PtSnNa/SUZ-4: An efficient catalyst for propane dehydrogenation. *Chin. J. Catal.* **2017**, *38*, 529–536. [[CrossRef](#)]
20. Shen, L.; Xia, K.; Lang, W.; Chu, L.; Yan, X.; Guo, Y. The effects of calcination temperature of support on PtIn/Mg(Al)O catalysts for propane dehydrogenation reaction. *Chem. Eng. J.* **2017**, *324*, 336–346. [[CrossRef](#)]
21. Gong, N.; Zhao, Z. Efficient supported Pt-Sn catalyst on carambola-like alumina for direct dehydrogenation of propane to propene. *Mol. Catal.* **2019**, *477*, 110543–110551. [[CrossRef](#)]
22. Vu, B.K.; Song, M.B.; Ahn, I.Y.; Suh, Y.W.; Suh, D.J.; Kim, J.S.; Shin, E.W. Location and structure of coke generated over Pt-Sn/Al<sub>2</sub>O<sub>3</sub> in propane dehydrogenation. *J. Ind. Eng. Chem.* **2011**, *17*, 71–76. [[CrossRef](#)]
23. Bare, S.R.; Vila, F.D.; Charochak, M.E.; Prabhakar, S.; Bradley, W.J.; Jaye, C.; Fischer, D.A.; Hayashi, S.T.; Bradley, S.A.; Rehr, J.J. Characterization of coke on a Pt-Re/γ-Al<sub>2</sub>O<sub>3</sub> re-forming catalyst: An experimental and theoretical study. *ACS Catal.* **2017**, *7*, 1452–1461. [[CrossRef](#)]
24. Nasution, P.S.; Jung, J.W.; Oh, K.; Koh, H.L. Coke combustion kinetics of spent Pt-Sn/Al<sub>2</sub>O<sub>3</sub> catalysts in propane dehydrogenation. *Korean J. Chem. Eng.* in press.
25. Li, B.; Xu, Z.; Chu, W.; Luo, S.; Jing, F. Ordered mesoporous Sn-SBA-15 as support for Pt catalyst with enhanced performance in propane dehydrogenation. *Chin. J. Catal.* **2017**, *38*, 726–735. [[CrossRef](#)]
26. Iglesias-Juez, A.; Beale, A.M.; Maaijen, K.; Weng, T.C.; Glatzel, P.; Weckhuysen, B.M. A combined in situ time-resolved UV-Vis, Raman and high-energy resolution X-ray absorption spectroscopy study on the deactivation behavior of Pt and PtSn propane dehydrogenation catalysts under industrial reaction conditions. *J. Catal.* **2010**, *276*, 268–279. [[CrossRef](#)]

27. Sun, C.; Luo, J.; Cao, M.; Zheng, P.; Li, G.; Bu, J.; Cao, Z.; Chen, S.; Xie, X. A comparative study on different regeneration processes of Pt-Sn/ $\gamma$ -Al<sub>2</sub>O<sub>3</sub> catalysts for propane dehydrogenation. *J. Energy Chem.* **2018**, *27*, 311–318. [[CrossRef](#)]
28. Xiong, H.; Lin, S.; Goetze, J.; Pletcher, P.; Guo, H.; Kovarik, L.; Artyushkova, K.; Weckuysen, B.M.; Datye, A.K. Thermally stable and regenerable platinum–tin clusters for propane dehydrogenation prepared by atom trapping on ceria. *Angew. Chem.* **2017**, *56*, 8986–8991. [[CrossRef](#)]
29. Pieck, C.L.; Vera, C.R.; Querini, C.A.; Parera, J.A. Differences in coke burning-off from Pt-Sn/Al<sub>2</sub>O<sub>3</sub> catalyst with oxygen or ozone. *Appl. Catal. A* **2005**, *278*, 173–180. [[CrossRef](#)]
30. Pieck, C.L.; Jablonski, E.L.; Parera, J.M. Regeneration of Coked Pt-Re/Al<sub>2</sub>O<sub>3</sub> catalyst by burning with oxygen and ozone. *Stud. Surf. Sci. Catal.* **1994**, *88*, 289–295.
31. Pieck, C.L.; Jablonski, E.L.; Parera, J.M. Sintering-Redispersion of Pt-Re/Al<sub>2</sub>O<sub>3</sub> during regeneration. *Appl. Catal.* **1990**, *62*, 47–60. [[CrossRef](#)]
32. Kim, G.H.; Jung, K.-D.; Kim, W.-I.; Um, B.-H.; Shin, C.-H.; Oh, K.; Koh, H.L. Effect of oxychlorination treatment on the regeneration of Pt-Sn/Al<sub>2</sub>O<sub>3</sub> catalyst for propane dehydrogenation. *Res. Chem. Intermed.* **2016**, *42*, 351–365. [[CrossRef](#)]
33. Artega, G.J.; Anderson, J.A.; Rochester, C.H. Effects of oxidation–reduction and oxychlorination–reduction cycles on CO adsorption by Pt-Sn/Al<sub>2</sub>O<sub>3</sub> catalysts. *J. Catal.* **1999**, *184*, 268–279. [[CrossRef](#)]
34. Lieske, H.; Völter, J. State of tin Pt-Sn/Al<sub>2</sub>O<sub>3</sub> reforming catalysts investigated by TPR and chemisorption. *J. Catal.* **1984**, *90*, 96–105. [[CrossRef](#)]
35. Geomar, J.A.; James, A.A.; Susanne, M.B.; Colin, H.R. Influence of oxychlorination treatment on the surface and bulk properties of a Pt-Sn/Al<sub>2</sub>O<sub>3</sub> catalyst. *J. Mol. Catal. A Chem.* **1999**, *145*, 183–201.
36. Merlen, E.; Beccat, P.; Bertolini, J.C.; Delichère, P.; Zanier, N.; Didillon, B. Characterization of bimetallic Pt-Sn/Al<sub>2</sub>O<sub>3</sub> Catalysts: Relationship between particle size and structure. *J. Catal.* **1996**, *159*, 178–188. [[CrossRef](#)]
37. Sexton, B.A.; Hughes, A.E.; Foger, K. An X-ray photoelectron spectroscopy and reaction study of Pt-Sn catalysts. *J. Catal.* **1984**, *88*, 466–477. [[CrossRef](#)]
38. Anresa, P.; Gaune-Escarda, M.; Brosa, J.P.; Hayerb, E. Enthalpy of formation of the (Pt-Sn) system. *J. Alloys Compd.* **1998**, *280*, 158–167. [[CrossRef](#)]
39. Kuznetsov, V.I.; Belyi, A.S.; Yurchenko, E.N.; Smolikov, M.D.; Protasova, M.T.; Zatulokina, E.V.; Duplyakin, V.K. Mössbauer spectroscopic and chemical analysis of the composition of Sn-containing components of Pt-Sn/Al<sub>2</sub>O<sub>3</sub>(Cl) reforming catalyst. *J. Catal.* **1986**, *99*, 159–170. [[CrossRef](#)]
40. Srinivasan, R.; Angelis, R.J.D.; Davis, B.H. Structural studies of Pt-Sn catalysts on high and low surface area alumina supports. *Catal. Lett.* **1990**, *4*, 303–308. [[CrossRef](#)]
41. Tasbihi, M.; Feyzi, F.; Amlashi, M.A.; Abdullah, A.Z.; Mohamed, A.R. Effect of the addition of potassium and lithium in Pt-Sn/Al<sub>2</sub>O<sub>3</sub> catalysts for the dehydrogenation of isobutane. *Fuel Process. Technol.* **2007**, *88*, 883–889. [[CrossRef](#)]
42. Llorca, J.; Delapiscina, P.R.; Fierro, J.L.; Sales, J.; Homs, N. Influence of metallic precursors on the preparation of silica-supported PtSn alloy—Characterization and reactivity in the catalytic activation of CO<sub>2</sub>. *J. Catal.* **1995**, *156*, 139–146. [[CrossRef](#)]
43. Srinivasan, R.; Davis, B.H. The structure of platinum-tin reforming catalysts. *Platin. Met. Rev.* **1992**, *36*, 151–163.
44. Vu, B.K.; Song, M.B.; Ahn, I.Y.; Suh, Y.W.; Suh, D.J.; Kim, W.; Koh, H.L.; Choi, Y.G.; Shin, E.W. Pt-Sn alloy phases and coke mobility over Pt-Sn/Al<sub>2</sub>O<sub>3</sub> and Pt-Sn/ZnAl<sub>2</sub>O<sub>4</sub> catalysts for propane dehydrogenation. *Appl. Catal. A* **2011**, *400*, 25–33. [[CrossRef](#)]
45. Sattler, J.J.H.B.; Ruiz-Martinez, J.; Santillan-Jimenez, E.; Weckhuysen, B.M. Catalytic dehydrogenation of light alkanes on metals and metal oxides. *Chem. Rev.* **2014**, *114*, 10613–10653. [[CrossRef](#)]
46. Nagaraja, B.M.; Shin, C.H.; Jung, K.D. Selective and stable bimetallic Pt-Sn/ $\theta$ -Al<sub>2</sub>O<sub>3</sub> catalyst for dehydrogenation of n-butane to n-butenes. *Appl. Catal. A* **2013**, *467*, 211–223. [[CrossRef](#)]
47. Hoang, D.L.; Farrage, S.A.-F.; Radnik, J.; Pohl, M.-M.; Schneider, M.; Lieske, H.; Martin, A. A comparative study of zirconia and alumina supported Pt and Pt-Sn catalysts used for dehydrocyclization of n-octane. *Appl. Catal. A* **2007**, *333*, 67–77. [[CrossRef](#)]

48. Song, A.; Lu, G. Enhancement of Pt–Ru catalytic activity for catalytic wet air oxidation of methylamine via tuning the Ru surface chemical state and dispersion by Pt addition. *RSC Adv.* **2014**, *4*, 15325–15331. [[CrossRef](#)]
49. Angel, G.D.; Bonilla, A.; Pena, Y.; Navarrete, J.; Fierro, J.L.G.; Acosta, D.R. Effect of lanthanum on the catalytic properties of PtSn/ $\gamma$ -Al<sub>2</sub>O<sub>3</sub> bimetallic catalysts prepared by successive impregnation and controlled surface reaction. *J. Catal.* **2003**, *219*, 63–73. [[CrossRef](#)]
50. Jung, J.W.; Kim, W.I.; Kim, J.R.; Oh, K.; Koh, H.L. Effect of direct reduction treatment on Pt-Sn/Al<sub>2</sub>O<sub>3</sub> catalyst for propane dehydrogenation. *Catalysts* **2019**, *9*, 446. [[CrossRef](#)]



© 2020 by the authors. Licensee MDPI, Basel, Switzerland. This article is an open access article distributed under the terms and conditions of the Creative Commons Attribution (CC BY) license (<http://creativecommons.org/licenses/by/4.0/>).